Surface code architecture for donors and dots in silicon with imprecise and non-uniform qubit couplings

G. Pica,[1] B. W. Lovett,[1] R. N. Bhatt,[2] T. Schenkel,[3] and S. A. Lyon[2]

[1]*SUPA, School of Physics and Astronomy, University of St Andrews, KY16 9SS, United Kingdom*
[2]*Dept. of Electrical Engineering, Princeton University, Princeton, New Jersey 08544, USA*
[3]*Ion Beam Technology Group, Lawrence Berkeley National Laboratory, Berkeley, CA 94720, USA*

Scaling entangling two-qubit operations based on the exchange interaction between spins in silicon to large quantum computers poses strict limitations to the placement of extremely coherent donors, while it is easily achieved with more fragile quantum dots. We present a surface code architecture where bismuth donors with long spin coherence times are coupled to electrons in quantum dots: All manipulations can be performed via microwave Rabi pulses, using well established techniques, while a robust, addressable SWAP gate between the donor and the dot states allows the pivotal operations for diagnosis of errors. The insensitivity of the entire scheme to the expected variations in the donor-dot coupling strength promises fast, fault-tolerant and massively parallel silicon quantum computing.

In 1998 Loss and DiVincenzo [1] showed how the exchange interaction between electron spins in semiconductor quantum dots could be harnessed for two-qubit operations, and Kane [2] presented a detailed plan in which the electron and nuclear spins of donor impurities in silicon, rather than dots, hold the qubits. In the intervening years a great deal of progress has been made in constructing donor-based [3–8] and dot-based quantum devices [9–13], but both approaches face significant fundamental hurdles, especially when considering scaling from individual devices to the large numbers required for a quantum computer. Here we show how bismuth donors in silicon can be combined with simple and readily controlled quantum dots to perform the operations required for implementing a two-dimensional surface code processor architecture [14]. This qubit technology combines the exceptional coherence and access to the nuclear degrees of freedom enjoyed by donors [15–17] with the more relaxed length-scales and demonstrated two-spin interactions of quantum dots [10–13]. Scalability is improved by using the exchange interaction only to swap quantum states through adiabatic transfer, rather than for entangling operations through accurate timing of dynamical gates: The fundamental advantage is that every multi-qubit manipulation required is robustly insensitive to even large variations in the donor-dot coupling.

In Fig. 1 we show an idealized diagram of a portion of the structure we are suggesting. Here we assume that the donors are incorporated below the quantum dots, and their interaction is controlled by a back-gate, as in the devices suggested by Schenkel *et al.* [18]. This vertical donor-dot configuration allows the dots to have quite simple gate structures and easily modeled electrostatic fields. We envision that several layers of metallization can be employed to form dense 2D arrays of quantum dots. Other arrangements have technological advantages and disadvantages which are discussed in the Supplemental Material (S1). The strong hyperfine mixing and large number of available states (nuclear spin I= 9/2) of the bismuth donors enables fast single- and two-qubit operations to be performed with high fidelity entirely within the manifold of donor states using microwave fields. Bi appears to be the best shallow donor for this application (see S2).

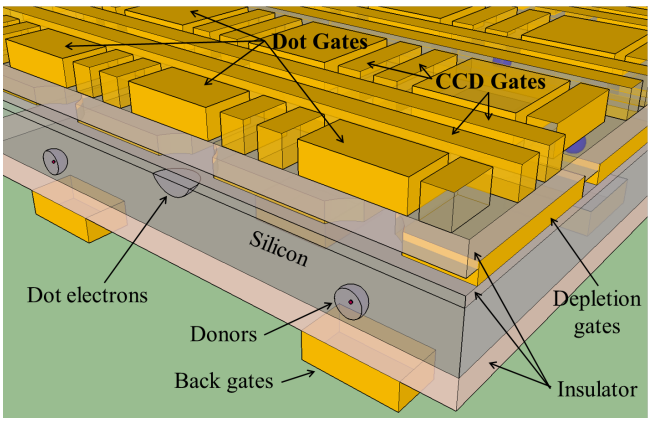

FIG. 1: Schematic diagram of the donor-dot array structure. The combination of top gates and holes in the depletion gate form the quantum dots, half of which are occupied with data qubit electrons. These electrons can be moved to dots positioned above the donor measurement qubits, each with a back gate to control the exchange coupling between the donor electron and the electron in the quantum dot.

The surface code architecture we will consider consists of a square planar array of qubits as described in detail by Fowler *et al.* [14]. We consider the data qubits (DQ) to be the spin of the electrons in the quantum dots, and the measurement qubits (MQ) to be states of the donor electron and nuclear spins (coupled through the hyperfine interaction). There are four basic operations which the qubit array must perform for error correction: (1) movement of the entire array of DQ to each of the four adjacent MQ in turn, (2) addressable CNOT operations with the DQ as control and the MQ as successive targets, (3) measuring the MQ, and (4) applying global Hadamard gates to the DQ. This protocol allows the diagnosis of phase-flip and bit-flip errors accumulating in the DQ array. The movement operation (1) would utilize the surface gates arranged, for example, as a 3-phase charge-coupled-device (CCD) array [19], as shown schematically in Fig. 1. When electrons are released from their quantum dots and allowed to move freely in a two-dimensional layer, it is known that

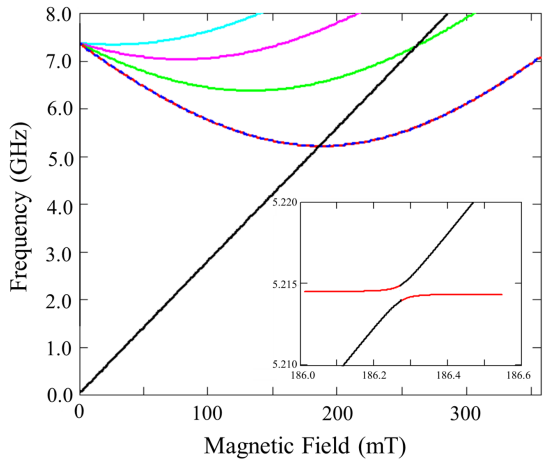

FIG. 2: Spin transition energies of neutral Si:Bi donors and an electron in a quantum dot in Si as a function of magnetic field. The dot and donor transition energies are nearly degenerate at the 5 GHz clock transition of the donor. Every donor curve represents two transitions, one 'allowed' and one 'forbidden' in the high field limit [24], whose separation is not resolved in the picture. The inset shows a calculation of the mixing between the 'allowed' and quantum dot transitions when the donor and dot are exchange coupled.

their spin coherence is significantly degraded, but still of the order of microseconds [20]. If the period of the donor-dot array is of order a micron, and the electrons are moved at 10^6 cm/s (about 500 mK electron energy in Si), the time to transport the electrons is only about 100ps. The error per qubit accumulated during the electron motion is about 10^{-4}, less than that which can be expected from gate operations. Higher fidelity motion can be expected if the transport channel forms a 1D quantum wire, or the electrons are transferred through a series of quantum dots [21]. The spin measurement operation (3) is always difficult, but high-fidelity measurement of single donors in Si has recently been demonstrated [3], even when the donor nuclear spin is involved [22]. For our purposes we will assume the existence of either a nondestructive spin readout technique for donors or the ability to reload a thermalized spin onto a donor after a readout that involves its ionization. The Hadamard operation (4) will use a global microwave field tuned to the quantum dot spin resonance frequency. Such operations can be performed with an infidelity of $< 10^{-3}$ [23].

The only lacuna in the implementation of a surface code is thus performing the CNOT gates between MQ and DQ, which we here construct via adiabatic transfer swaps based on the exchange coupling between the donor and its paired dot electron (see Fig. 1). These SWAP operations are controlled by gate voltages on a site-by-site basis, allowing all other operations to be applied globally; crucially, they retain fault-tolerant fidelity even when the donor-dot exchange interaction strength varies widely from device to device.

The transition energy of the donor and dot spin states as a function of applied magnetic field is shown in Fig. 2, where it is assumed that the exchange coupling between the donor

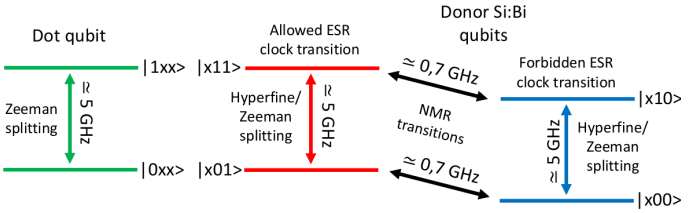

FIG. 3: Diagram of the transition energies and coupling of the three qubits in a donor-dot structure. The 'Dot' and 'ESR' qubits both have transition frequencies of about 5 GHz (the lowest clock transition of Si:Bi), while the 'NMR' qubit frequency is about 0.74 GHz. The Dot qubit and the allowed transition of the ESR qubit ($|\mathrm{NMR}\rangle = |1\rangle$) can be coupled by a gate-controlled exchange interaction.

and dot electrons is initially zero. We propose addressing the donor 'clock transitions' which have a frequency that is not sensitive to magnetic field to first order [7], and thus can cross the quantum dot transition whose frequency is simply linear in the magnetic field. In Fig. 2 it is shown that the dot transition crosses the lowest donor transition almost exactly at its minimum, where the spins have particularly long lived coherence. As shown in S2 there will always be a crossing at the lowest clock transition when the nuclear spin is 9/2, or larger.

Electron spin resonance (ESR) measurements of the clock transition near 5 GHz have shown that there are two nearly degenerate components at every clock transition [7, 24]. Since they involve different initial and final states, these four states can be used as two independent qubits residing on the bismuth. It is convenient to label the upper of each pair of transitions 'forbidden' and the lower 'allowed', even though this is exact only in the high field limit (where Zeeman splitting is much larger than hyperfine energy).

Among the 20 distinct states between the $I = 9/2$ nucleus and $S = 1/2$ electron of bismuth, here we will only use the two nearly degenerate qubits at the clock transitions. The inset in Fig. 2 shows the calculated transition energies near the 5 GHz clock transition when a nonzero exchange coupling between the dot electron and the donor electron is turned on. There is an avoided crossing with the allowed donor transition, as one might expect. As discussed in S4, there is no avoided crossing with the forbidden transition: This enables a three-qubit controlled-SWAP operation (Fedkin gate [25]) to be performed naturally.

In Fig. 3 we schematically summarize the three qubits (see also S4). The first (left) is the electron spin in the dot, and given the name 'Dot' qubit. The magnetic field will be held near the exchange induced avoided crossing at the 5 GHz clock transition. The dot qubit can be driven by conventional microwave ESR fields. The second qubit consists of the donor states at the 5 GHz clock transition. In the high-field limit this qubit would be simply an electron spin on the donor, and thus we call it the 'ESR' qubit. The third qubit is the coupled electron and nuclear states making up the allowed versus the forbidden transitions. In the high field limit this would just be a nuclear spin, and we call it the 'NMR' qubit. The transition

energy of this qubit is only about 0.74 GHz.

The basic operation of the donor-dot device can now be described: We assume that the dots contain the DQ and the $|\text{ESR}\rangle$ qubits have been initialized in a $|0\rangle$ state. The transfer gates bring the appropriate data electron to the quantum dot situated above the donor. The magnetic field will be held below that corresponding to the (anti-)crossing of the dot and donor transitions (inset of Fig. 2). Pulsing the backgate voltage below the donor adiabatically turns on an exchange coupling between the donor and the dot. Sweeping the magnetic field through the resulting avoided crossing swaps the $|101\rangle$ and $|011\rangle$ states (linked by an allowed ESR transition), but not the corresponding states with $|\text{NMR}\rangle = |0\rangle$ (i.e. $|100\rangle$ and $|010\rangle$, linked by a forbidden ESR transition). The subset of donor-dot pairs taking part in this SWAP operation, which we will call $\mho$, is addressed by selectively energizing the appropriate backgates – hence a site-selective SWAP.

With the DQ swapped to the ESR state of the donor, microwaves can drive a transition on the ESR qubit, conditioned on the state of the NMR qubit. This conditional excitation Π_{ESR} is nothing more than pulsed Electron Nuclear Double Resonance (pulsed ENDOR) [26]. These CNOT fields are applied globally, since those sites where the SWAP was not done will have their ESR qubit initialized to $|0\rangle$, and the CNOT has no effect. The strong hyperfine mixing near the clock transitions in Si:Bi allows the ENDOR transitions to be driven through the electronic part of the states, and thus can be as fast as conventional ESR pulses [24]. Following the CNOT operation the exchange interaction can be reestablished and the ESR qubit swapped back to the dot electron: The overall result is a CNOT with the NMR qubit as control and Dot qubit as target. This gate can be turned into the basic operation required to maintain the surface code, i.e. a CNOT with the data qubit as control and the MQ as target, via the application of four Hadamard gates $\mathcal{H}_i$ (see S5):

$$\text{Surface code CNOT} = \mathcal{H}_{\text{dot}}\mathcal{H}_{\text{NMR}}\mho\Pi_{\text{ESR}}\mho^{-1}\mathcal{H}_{\text{dot}}^{-1}\mathcal{H}_{\text{NMR}}^{-1}. \quad (1)$$

After each DQ has been moved to perform a CNOT with its four neighboring donors, the spin state of those donors must be measured then reinitialized, and a similar protocol (without the Hadamard gates in Eq. 1) performed for the X stabilizer measurement.

One subtlety arises concerning the length of the selective ENDOR pulses. The splitting between the allowed and forbidden transitions is only about 2 MHz, while selectively exciting one and not the other is a building block of the CNOT gate. Therefore if the difference in transition energy provides the only selectivity, the pulses can be no shorter than about 250 ns to avoid exciting the other transition. However, these transitions are excited by opposite helicities of the microwave photons[24], and photon polarization can be used to excite them selectively with short pulses.

The protected quantum memory designed so far could be easily endowed with defects and braiding, that allow the definition of logical qubits within a surface code [27]. To form a defect at any donor site the stabilizer operations are blocked by not applying the voltage to that bottom gate: Thus the exchange interaction and SWAP is disabled. The other quantum gates in Eq. 1 either only affect the donor qubits, which are reset anyway by the measurement step, or are pairs of Hadamard gates, which reduce to the identity.

The electrons in silicon occupy conduction band valleys at large wavevector k, which means their wavefunctions oscillate rapidly in space. This feature gives rise to rapid variations in the strength of the exchange interaction between pairs of donors as their separation changes [28], making the high-fidelity dynamical gates proposed for donor-based quantum computers [2] difficult to engineer [29]. More recent calculations have shown that the depth of the exchange oscillations are not as severe as originally predicted [30] but there are significant variations, nonetheless. Moving electrons from one donor to another has been suggested as an alternative to exchange-based entanglement of nuclear spins of donors [31, 32], but with hyperfine interaction frequencies of order 100 MHz or higher, controlling the timing of the electron removal and reintroduction to the donors becomes problematic.

A key feature of the approach we present here is that the exchange interaction J between a donor and a quantum dot is only used for our adiabatic swapping operation, which is intrinsically robust against the expected oscillations in J as the position of the donor changes with respect to the abrupt heterointerface where the quantum dot is formed. In Fig. 4(a) we show a multi-valley effective mass theory [33] calculation of the exchange energy of a donor and dot electron as a function of the distance from the surface to the donor ion, assuming a field of 4 kV/cm is confining the dot electron. It is clear that moving the donor one lattice constant closer or farther from the surface can bring the exchange interaction from a peak to a trough.

The placement of phosphorus donors in a single plane has been demonstrated, but that technique relies on the particular chemistry of hydrogen-terminated silicon and PH_3 in ultra-high vacuum [34]. Locating a Bi donor precisely on the scale of a lattice constant has not been demonstrated and placement of Bi donors by ion implantation is associated with larger alignment uncertainties [18]. Thus quantum gates utilizing the exchange interaction either must be individually tuned (by setting gate voltages) at each donor-dot site, or, as we now exemplify, possess an innate insensitivity to the strength of the interaction.

In order to achieve such an insensitivity the population transfer between the $|011\rangle$ and $|101\rangle$ states, the manipulation at the core of the operation $\mho$, is performed adiabatically: The magnetic field is swept through the avoided crossing, while at the same time the backgate below that donor is adiabatically positively biased to cause the dot and donor wavefunctions to overlap. In S3 we show that it is sufficient to ramp the voltage up by about 10 mV to increase the exchange coupling by three orders of magnitude for typical device parameters,

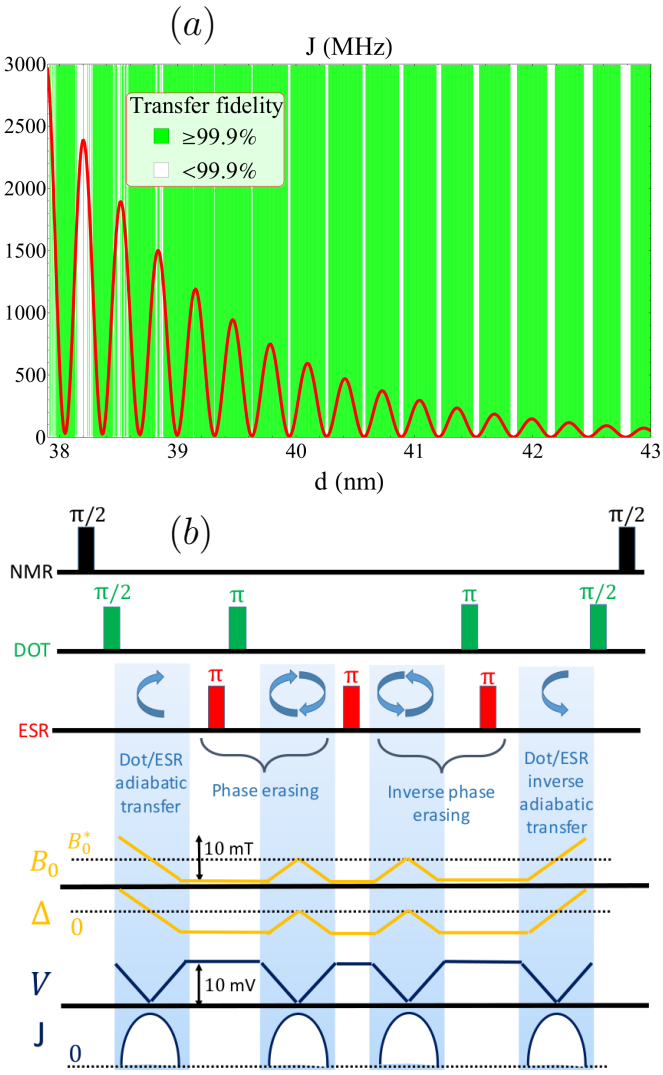

FIG. 4: (a) The red line shows a best fit to a set of calculations of exchange splittings that the different donor-dot pairs of electrons would experience within a scaled architecture, due to the imprecise implantation depth d of the donors (an equivalent applied electric field $F = 4\,\mathrm{kV/cm}$ is assumed). The pairs within the green regions will undergo adiabatic population transfer with fidelity higher than 99.9%. These regions become thinner to the left edge of the plot, where the high couplings break the adiabaticity condition, and to the right edge, where the couplings are too weak to induce an efficient depopulation at the avoided crossing. (b) Complete CNOT sequence between the Dot and the NMR qubit, that includes performing resonant Hadamard ($\pi/2$) and π Rabi pulses on the different qubits, plus adiabatic Dot/ESR transfer sequences $\mho$ (light blue boxes) based on linear dc tunings of the magnetic field B_0 and the backgate voltage V. The simple adiabatic transfers take place thanks to the J coupling turned on at the crossing points of the Dot/ESR levels ($\Delta = 0$), while 'phase erasing' steps allow the final quantum state to be independent from the evolution induced by each exact J magnitude. All operations require a few μs.

thus enabling the population transfer. The adiabaticity of this manipulation is achieved if $\hbar\dot{J} \ll \Delta_0^2$, where Δ_0 corresponds to the initial energy difference between the two states, which is limited by the experimental ability to sweep the dc global magnetic field B_0. Larger magnetic field excursions would give slower gates: We assume that $10\,\mathrm{mT}$ sweeps can be realized within $1\,\mu\mathrm{s}$. It has been demonstrated that the backgate voltage could be easily switched by the required amount within this time window [35], leading to effective population transfer within a realistic operational framework. Fig. 4(a) shows simulated adiabatic transfer fidelities that are higher than 99.9%, well within the 1% error rate per operation tolerated by the surface code [14], across two orders of magnitude of the donor-dot exchange coupling. This is a conservative estimate of the calculated range of interactions that the pairs could experience across an array like Fig. 1.

The naive execution of an adiabatic transfer as described so far could lead to unwanted residual entanglement between the data and the measurement qubits, as a result of large J-dependent phases built up during the non-trivial dynamics. In Fig. 4(b) we show how the population transfer between $|011\rangle$ and $|101\rangle$ can be turned into a SWAP times a Z-phase gate between the same states, which we call our $\mho$ gate, *independent of the precise magnitude of the J coupling*. This is achieved via extra phase-erasing steps that involve π-Rabi transitions on the Dot and ESR qubits followed by adiabatic dc tuning of magnetic field and backgate voltage (see S5).

In summary, we have shown how bismuth donors and quantum dots in a silicon host can be combined into a surface code quantum computer architecture. Microwave driven ENDOR transitions are high fidelity two-qubit gates on the bismuth donors. Rather than turning an exchange interaction on and off to generate a dynamical phase, exchange is used to swap spin states between the quantum dots and the donors through adiabatic transfer. These SWAP gates are insensitive to order-of-magnitude variations in the interaction strength, and thus allow high fidelity surface code CNOTs for all donor-dot pairs. The insensitivity to donor-dot alignment variations (see S3) may enable fabrication of donor-dot pairs in large arrays by ion implantation [18]. The only required site-selective operation required is the control of the exchange based swap between the donors and the dots, which is accomplished simply with a gate voltage, whereas other approaches require tuning individual qubits in or out of resonance with a global microwave field [2]. The nearest-neighbor coupling required to implement the surface code could be achieved by shuttling the array of electrons with CCD-like gates. The minimum pitch of an array of these donor-dot devices would only be limited by the CCD gates, and submicron periods are technically feasible. With micron pitch structures the surface code would have 10^8 physical qubits per square centimeter, allowing for many error-corrected logical qubits.

This research was funded by the joint EPSRC (EP/I035536)/ NSF (DMR-1107606) Materials World Network grant (GP, BWL, SAL), the EPSRC grant EP/K025562 (BWL), the NSF MRSEC grant DMR-01420541 (SAL), and the Department of Energy, Office of Basic Energy Sciences grant de-sc0002140 (RNB) and the DOE Office of Science under contract no. DE-AC02-05CH11231 (TS). GP thanks the University of St Andrews and EPSRC for a

Doctoral Prize Fellowship.

[1] D. Loss and D. P. DiVincenzo, Phys. Rev. A **57**, 120 (1998).

[2] B. E. Kane, Nature **393**, 133 (1998).

[3] A. Morello, J. J. Pla, F. A. Zwanenburg, K. W. Chan, K. Y. Tan, H. Huebl, M. Möttönen, C. D. Nugroho, C. Y. Yang, J. A. van Donkelaar, A. D. C. Alves, D. N. Jamieson, C. C. Escott, L. C. L. Hollenberg, R. G. Clark, and A. S. Dzurak, Nature **467**, 687 (2010).

[4] J. J. Pla, K. Y. Tan, J. P. Dehollain, W. H. Lim, J. J. L. Morton, D. N. Jamieson, A. S. Dzurak, and A. Morello, Nature **489**, 541 (2012).

[5] A. M. Tyryshkin, S. Tojo, J. J. L. Morton, H. Riemann, N. V. Abrosimov, P. Becker, H.-J. Pohl, T. Schenkel, M. L. W. Thewalt, K. M. Itoh, and S. A. Lyon, Nat. Mater. **11**, 143 (2012).

[6] J. T. Muhonen, J. P. Dehollain, A. Laucht, F. E. Hudson, R. Kalra, T. Sekiguchi, K. M. Itoh, D. N. Jamieson, J. C. McCallum, A. S. Dzurak, and A. Morello, Nat. Nanotechnol. **9**, 986 (2014).

[7] G. Wolfowicz, A. M. Tyryshkin, R. E. George, H. Riemann, N. V. Abrosimov, P. Becker, H.-J. Pohl, M. L. W. Thewalt, S. A. Lyon, and J. J. L. Morton, Nature Nanotechnology **8**,1 561 (2013).

[8] H. Büch, S. Mahapatra, R. Rahman, A. Morello, and M. Y. Simmons, Nature Communications **4**, 2017 (2013).

[9] H. Bluhm, S. Foletti, I. Neder, M. Rudner, D. Mahalu, V. Umansky, and A. Yacoby, Nature Physics **7**, 109 (2010).

[10] B. M. Maune, M. G. Borselli, B. Huang, T. D. Ladd, P. W. Deelman, K. S. Holabird, A. A. Kiselev, I. Alvarado-Rodriguez, R. S. Ross, A. E. Schmitz, M. Sokolich, C. A. Watson, M. F. Gyure, and A. T. Hunter, Nature **481**, 344 (2012).

[11] J. R. Petta, A. C. Johnson, J. M. Taylor, E. A. Laird, A. Yacoby, M. D. Lukin, C. M. Marcus, M. P. Hanson, and A. C. Gossard, Science **309**, 2180 (2005).

[12] J. R. Prance, Z. Shi, C. B. Simmons, D. E. Savage, M. G. Lagally, L. R. Schreiber, L. M. K. Vandersypen, M. Friesen, R. Joynt, S. N. Coppersmith, and M. A. Eriksson, Phys. Rev. Lett. **108**, 046808 (2012).

[13] M. Veldhorst, C. H. Yang, J. C. C. Hwang, W. Huang, J. P. Dehollain, J. T. Muhonen, S. Simmons, A. Laucht, F. E. Hudson, K. M. Itoh, A. Morello, and A. S. Dzurak, ArXiv e-print 1411.5760 (2014).

[14] A. G. Fowler, M. Mariantoni, J. M. Martinis, and A. N. Cleland, Phys. Rev. A **86**, 032324 (2012).

[15] K. Saeedi, S. Simmons, J. Z. Salvail, P. Dluhy, H. Riemann, N. V. Abrosimov, P. Becker, H.-J. Pohl, J. J. L. Morton, and M. L. W. Thewalt, Science **342**, 830 (2013).

[16] D.R. McCamey, J. Van Tol, G. W. Morley, and C. Boehme, Science **330**, 1652 (2010).

[17] J. J. L. Morton, A. M. Tyryshkin, R. M. Brown, S. Shankar, B. W. Lovett, A. Ardavan, T. Schenkel, E. E. Haller, J. W. Ager, and S. A. Lyon, Nature **455**, 1085 (2008).

[18] T. Schenkel, C. Lo, C. Weis, J. Bokor, A. Tyryshkin, and S. Lyon, in *Single-Atom Nanoelectronics*, E. Prati and T. Shinada (eds.), (Panstanford Publishing, Singapore, 2013), chapter 11, ArXiv e-print 1110.2228.

[19] Y. Ono, A. Fujiwara, K. Nishiguchi, H. Inokawa, and Y. Takahashi, J. Appl. Phys. **97**, 031101 (2005).

[20] A. M. Tyryshkin, S. A. Lyon, W. Jantsch, and F. Schäffler, Phys. Rev. Lett. **94**, 126802 (2005).

[21] S. Oh, L.-A. Wu, Y.-P. Shim, J. Fei, M. Friesen, and X. Hu, Phys. Rev. A **84**, 022330 (2011).

[22] J. J. Pla, K. Y. Tan, J. P. Dehollain, W. H. Lim, J. J. L. Morton, F. A. Zwanenburg, D. N. Jamieson, A. S. Dzurak, and A. Morello, Nature **496**, 334 (2013).

[23] J. T. Muhonen, A. Laucht, S. Simmons, J. P. Dehollain, R. Kalra, F. E. Hudson, S. Freer, K. M. Itoh, D. N. Jamieson, J. C. McCallum, A. S. Dzurak, and A. Morello, J. Phys.: Condens. Matter **27**, 154205 (2015).

[24] G. W. Morley, M. Warner, A. M. Stoneham, P. T. Greenland, J. van Tol, C. W. M. Kay, and G. Aeppli, Nature Materials **9**, 725 (2010).

[25] E. Fredkin and T. Toffoli, International Journal of Theoretical Physics **21**, 219 (1982).

[26] G. Feher, Phys. Rev. **103**, 834 (1956).

[27] C. Horsman, A. G. Fowler, S. Devitt, and R. Van Meter, New J. Phys. **14**, 123011 (2012).

[28] K. Andres, R. N. Bhatt, P. Goalwin, T. M. Rice, and R. E. Walstedt, Phys. Rev. B **24**, 244 (1981).

[29] B. Koiller, X. D. Hu, and S. Das Sarma, Phys. Rev. Lett. **88**, 027903 (2002).

[30] G. Pica, B. W. Lovett, R. N. Bhatt, and S. A. Lyon, Phys. Rev. B **89**, 235306 (2014).

[31] B. E. Kane, Fortschritte der Physik **48**, 1023 (2000).

[32] J. J. L. Morton, ArXiv e-print 0905.4008 (2009).

[33] G. Pica, G. Wolfowicz, M. Urdampilleta, M. L. W. Thewalt, H. Riemann, N. V. Abrosimov, P. Becker, H.-J. Pohl, J. J. L. Morton, R. N. Bhatt, S. A. Lyon, and B. W Lovett, Phys. Rev. B **90**, 195204 (2014).

[34] M. Fuechsle, J. A. Miwa, S. Mahapatra, H. Ryu, S. Lee, O. Warschkow, L. C. L. Hollenberg, G. Klimeck, and M. Y. Simmons, Nature Nanotechnology **7**, 242 (2012).

[35] Z. Shi, C. B. Simmons, D. R. Ward, J. R. Prance, R. T. Mohr, T. S. Koh, J. K. Gamble, X. Wu, D. E. Savage, M. G. Lagally, M. Friesen, S. N. Coppersmith, and M. A. Eriksson, Phys. Rev. B **88**, 075416 (2013).

Supplementary Information for 'Surface code architecture for donors and dots in silicon with imprecise and non-uniform qubit couplings'

S1. LAYOUT AND OPERATIONAL CONSIDERATIONS

For clarity, in the main text we have considered one particular mode of operation and arrangement of donors and dots, but there are a number of other similar architectures which have advantages and disadvantages. Here we discuss some of these other possibilities, as well as our current understanding of their strengths and weaknesses.

In Fig. 1 of the main text we have shown a diagram of a donor/dot array in which the exchange interaction is controlled by a back gate below the donors. However, a fully planar arrangement in which the donors are closer to the Si/SiO_2 interface and couple laterally to the dots, as suggested by Carroll and coworkers [1] may be preferable from a fabrication viewpoint. This approach would be closest to current practice for classical silicon circuits, and it would eliminate the need for complex device layers contacted from both sides. However, for operations such as a logical Hadamard, it would be advantageous for the donor electrons to be able to be moved across more than one site. Measuring the donors if they are in the same layer as the dots could also lead to a complex routing arrangement for moving electrons to the neighboring donors. It should be noted that multi-layer heterogeneous integration with micron-scale device registration, as would be necessary for the backgate approach, has been demonstrated [2]. Details of layout and fabrication complexity will determine this choice, and are beyond the scope of the present discussion.

Single-qubit operations on the surface code involve applying gates to subsets of the data qubits. In this architecture the appropriate subset is chosen by selectively swapping to the donors and performing the qubit rotations on them. It would be possible for the measurement donors to do double-duty for the single spin gates, but it may be advantageous to associate a donor with every quantum dot, rather than just the measurement sites, to aid in these operations. Also, we have discussed measuring and reinitializing a subset of the donors at each step, though measuring all of the donors each time and simply ignoring the unnecessary results would probably be preferable to minimize decoherence.

A further consideration is whether to use the dot electrons as data qubits and the donors for measurement, or the other way around. There is no particular advantage in terms of the quantum gates, since global single qubit operations can transform the operations appropriately. Fast efficient single spin measurement and initialization are required for surface codes, as for other methods of quantum error correction. Spin to charge conversion for spin measurement has been ubiquitous in quantum dot qubit experiments for over a decade [3], while direct spin-dependent tunneling for single donor spin readout is a more recent development [4]. Spin-selective optical excitation of donors may relax requirements on electron temperature [5], and optical readout of single donors has been shown [6]. However, the spin readout method is also connected to the arrangement of the donor/dot array. If the donors are the measurement qubits, all of the donor gates and readout devices (single-electron transistors (SETs) [7] or quantum point contacts [8] to sense single charges) can be integrated onto the back side of the array. The transfer gates on the top of the array have a simple structure with this approach. However, if spin readout is through the dots, then the quantum point contacts (or SETs) for sensing the charge would typically be placed on the surface next to the dots, and the transport of the dot electrons to the nearest neighbor donors becomes more difficult.

S2. CHOICE OF DONOR

Si:Bi systems have now been experimentally established as excellent candidate qubits [9]. Bi 9/2 nuclear spins combined with the 1/2 donor electron spins provide a rich Hilbert space of states from which to choose the qubit logical $|0\rangle$ and $|1\rangle$. Their hyperfine interaction is the strongest available among the group V substitutional donors in Si, which makes it easier to transfer the information from the electron to the nuclear spin; moreover, it allows the existence of so-called clock transitions [10], i.e. transitions between hyperfine mixed nuclear-electron spin states that are very insensitive to the actual magnetic field of the environment. We will now identify the specific donor states that host the measurement qubits that we propose to couple to the dot data qubits within the surface code.

The mixed Hilbert space set up by the electron and nuclear spin levels of a group V donor is governed, in the presence of a fixed magnetic field $\mathbf{B}_0$, by the Hamiltonian

$$H = \gamma_e \mathbf{B}_0 \cdot \mathbf{S} - \gamma_n \mathbf{B}_0 \cdot \mathbf{I} + A\, \mathbf{S} \cdot \mathbf{I}, \tag{S1}$$

where A is the hyperfine interaction between the nuclear spin $\mathbf{I}$ and the electron spin $\mathbf{S}$, $\gamma_e = \frac{g_e \mu_B}{\hbar} = 27.997\,\text{GHz/T}$ is the magnetic moment of the electron, $\gamma_n = 0.007\,\text{GHz/T}$ is the nuclear magnetic moment.
The behaviour of the corresponding spectrum in the region of intermediate $\mathbf{B}_0$ (roughly speaking, when $A \approx \gamma_e B_0$) can get very interesting, if I is large enough. In fact, apart from Si:P, the manifold of the mixed levels for all group V donors (As, ^{111}Sb, ^{113}Sb, and Bi with respective I=3/2, 5/2, 7/2, 9/2) allows for specific values of B_0, where the energy difference f between selected mixed eigenstates has a minimum, i.e. $\frac{\partial f}{\partial B_0} = 0$ [11]. The immediate and useful consequence of such rich behaviour, conceptually due to the large number of mixed levels available, is that the T_2 of a qubit stored in the two donor levels separated by a 'clock transition' will not suffer from local fluctuations in the magnetic field, which include hyperfine and dipolar interaction with the ^{29}Si nuclei and paramagnetic coupling to other electrons and impurities.
The eigenstates of Eq. S1 can be expressed as [12]

$$|\pm, m\rangle = a_m^{\pm}|\pm 1/2, m \mp 1/2\rangle + b_m^{\pm}|\mp 1/2, m \pm 1/2\rangle, \tag{S2}$$

where

$$a_m^{\pm} = \begin{cases} \cos(\theta_m/2) \\ -\sin(\theta_m/2) \end{cases}, \; b_m^{\pm} = \begin{cases} \sin(\theta_m/2) \\ \cos(\theta_m/2) \end{cases} \tag{S3}$$

and

$$\theta_m = \arctan\left[\frac{A\sqrt{I(I+1)+\frac{1}{4}-m^2}}{(Am + B_0\gamma_e + B_0\gamma_n)}\right], \;\; 0 \le \theta_m < \pi, \tag{S4}$$

while the corresponding eigenenergies are

$$E_m^{2\pm} = -\frac{A}{4} - B_0\gamma_n m \pm \sqrt{A^2[I(I+1)+\frac{1}{4}-m^2] + (Am + B_0\gamma_e + B_0\gamma_n)^2}, \tag{S5}$$

for $-I - 1/2 < m < I + 1/2$, and

$$E_m^{1\pm} = \pm\frac{1}{2}(Am + B_0\gamma_e + B_0\gamma_n) - \frac{1}{4}(A + 4B_0\gamma_n m), \tag{S6}$$

for $m = \pm(I + 1/2)$.
In a regime of intermediate $\mathbf{B}_0$ values, large mixing between $|m_S\rangle$ and $|m_I\rangle$ states ensues that allowed GHz transitions occur between states of the form $|\pm, m\rangle \leftrightarrow |\pm, m-1\rangle$ and $|\pm, m\rangle \leftrightarrow |\mp, m-1\rangle$. It has been observed experimentally [12] and then clarified theoretically [11] that the sweet spots aforementioned occur for the second kind of transitions, namely when:

$$B_0 = B_0^* \approx -\frac{A}{\gamma_e}\frac{(m-1)\sqrt{I(I+1)+\frac{1}{4}-m^2} + m\sqrt{I(I+1)+\frac{1}{4}-(m-1)^2}}{\sqrt{I(I+1)+\frac{1}{4}-m^2} + \sqrt{I(I+1)+\frac{1}{4}-(m-1)^2}}, \tag{S7}$$

with the restriction -I+3/2 $\le m \le 0$. The nature of the expression S7 should clarify why Si:P does not show any clock transition, while their number increases for larger I, as there will be more integers $m \le 0$ able to satisfy such condition.
Since our final goal is to 'hybridize' an highly coherent donor system with the two Zeeman split states of a quantum dot electron spin, we would like the Zeeman dot frequency $f_{\text{dot}} \approx B_0\gamma_e$ (the dot electron g-factor is 1.997) to cross some donor clock transition f_{donor} at the sweet spot where $\frac{\partial f}{\partial B_0} = 0$, as shown in Fig. 2 of the main text. Let us show that meeting those requirements automatically selects Si:Bi as the only option among group V donors in silicon: after rearranging Eq. S7, we get

$$f_{\text{dot}} = \gamma_e B_0^* \approx -A\left(m - (1 + \frac{2m-1}{I(I+1)+\frac{1}{4}-m^2})^{-1/2}\right) < -A(m-1). \tag{S8}$$

On the other hand, close to a clock transition, the eigenenergies of the hybrid states involved can be approximated as

$$E_m^{2\pm} \approx -\frac{A}{4} \pm \frac{A}{2}\sqrt{I(I+1)+\frac{1}{4}-m^2}. \tag{S9}$$

Hence, requiring that a $|\pm, m\rangle \leftrightarrow |\mp, m-1\rangle$ transition is degenerate with f_{dot} implies

$$f_{\text{donor}} - f_{\text{dot}} = \frac{A}{2}\left(\sqrt{I(I+1)+\frac{1}{4}-m^2}+\sqrt{I(I+1)+\frac{1}{4}-(m-1)^2}\right) - \gamma_e B_0^* = 0. \tag{S10}$$

By virtue of S8,

$$f_{\text{donor}} - f_{\text{dot}} > \frac{A}{2}\left(\sqrt{I(I+1)+\frac{1}{4}-m^2}+\sqrt{I(I+1)+\frac{1}{4}-(m-1)^2}\right) + A(m-1), \tag{S11}$$

and this latter expression is seen to be always positive unless $m \leq -3$. Thus the required degeneracy can be achieved only within Si:Bi, specifically addressing the $|+, m=-3\rangle \rightarrow |-, m=-4\rangle$ transition, called allowed transition in the main text, and the $|+, m=-4\rangle \rightarrow |-, m=-3\rangle$ transition, the forbidden one. The following hybrid electron-nuclear spin states are respectively involved (the colored arrows label the qubit transitions as indicated in Fig. 3 in the main text):

$$\begin{array}{cc}
\cos\frac{\theta_{-3}}{2}|1/2,-7/2\rangle + \sin\frac{\theta_{-3}}{2}|-1/2,-5/2\rangle & -\sin\frac{\theta_{-3}}{2}|1/2,-7/2\rangle + \cos\frac{\theta_{-3}}{2}|-1/2,-5/2\rangle \\
f_{\text{donor}} = 5.2142\,\text{GHz} \quad \downarrow \quad B_0^* = 0.188179\text{T} & f_{\text{donor}} = 5.216\,83\,\text{GHz} \quad \uparrow \quad B_0^* = 0.188086\text{T} \\
-\sin\frac{\theta_{-4}}{2}|1/2,-9/2\rangle + \cos\frac{\theta_{-4}}{2}|-1/2,-7/2\rangle & \cos\frac{\theta_{-4}}{2}|1/2,-9/2\rangle + \sin\frac{\theta_{-4}}{2}|-1/2,-7/2\rangle.
\end{array} \tag{S12}$$

The occurrence of an energy crossing between the Zeeman transition linking the two dot electron spin states and the allowed donor clock transition is displayed in Fig. 2 in the main text. In the high field limit (Zeeman much larger than hyperfine) the right transition in Eq. S12 is forbidden, since it involves a nuclear spin flip: this is the motivation for labeling the left transitions as 'allowed' and the right as 'forbidden', even though both are actually enabled in the intermediate B_0 regime investigated here. Each of these two transitions couples to opposite helicity microwave photons, as noted by Ref. [13], thus the selective excitation of a single transition in the pair does not pose fundamental physical limitations, even though the energy difference between the two, about 2 MHz, would hardly be distinguished with fast microwave pulses.

S3. EXCHANGE COUPLING BETWEEN A MOS QUANTUM DOT AND A Si:Bi DONOR

The aim of this Section is to evaluate the exchange coupling that would arise between an electron spin which is confined in a quantum dot close to a Si/SiO_2 interface and the excess electron spin provided by a donor Bi atom implanted deep in the bulk of a Si layer, at a distance d from the interface. This interaction paves the way for the fundamental data-measurement qubit coupling that is needed for the surface code proposed in the main text.

The confinement for the interface electron is provided by an external electric field F (in the $\hat{z}$ direction, which we assume to be perpendicular to the plane which contains the interface) and by a quantum dot potential (approximately parabolic) in the transverse $x-y$ plane. This simple modeling accounts for the voltage landscape that the confining interface gates would be able to produce. The impurity potential due to the substitutional implanted Bi atom completes the description of this two-electron problem: the potential energy of an electron in this system, as shown in Fig. S1, is described as:

$$V(\mathbf{r}) = +eFz - \frac{e^2}{\epsilon_{Si}\sqrt{\rho^2+z^2}}(1 - e^{-b\sqrt{\rho^2+z^2}} + B\sqrt{\rho^2+z^2}e^{-b\sqrt{\rho^2+z^2}}) + \frac{e^2 Q}{\epsilon_{Si}\sqrt{\rho^2+(z+2d)^2}} - \frac{e^2 Q}{4\epsilon_{Si}(z+d)} + \frac{\omega_0}{2}\rho^2, \tag{S13}$$

where $\epsilon_{Si} = 11.4$ is the dielectric constant of Silicon, b and B are two pseudopotential parameters that mimic the Si:Bi impurity potential outside the donor central cell [14], ρ is the radial coordinate in the plane of the interface, $Q = \frac{\epsilon_{SiO_2} - \epsilon_{Si}}{\epsilon_{SiO_2} + \epsilon_{Si}}$ is a factor to parametrize the electrostatic image effects due to the dielectric barrier, d is the distance of the nucleus from the interface, ω_0 simulates the dot confining gates. The infinite wall at the interface models the $\approx 3\,\text{eV}$ step between the energies of the conduction band edges of the silicon and the oxide layer, and implements our assumption that the dot electron state does not penetrate significantly into the oxide. The electric field is assumed to be uniform and unidirectional throughout the system, which is a reasonable approximation for realistic devices of this kind, as is the parabolic transverse confinement that binds the quantum dot. We take into account the effect of the accumulation of charges on the dielectric SiO_2 boundary, induced by the electrostatic configuration in the Si layer, via the image-charge method [15].

Effective mass theory is used in our evaluations of exchange splittings, since the latter will gain the most relevant contributions from the electronic densities in the intermediate spatial region between the two wells, i.e. far from the Bi nuclear cell where

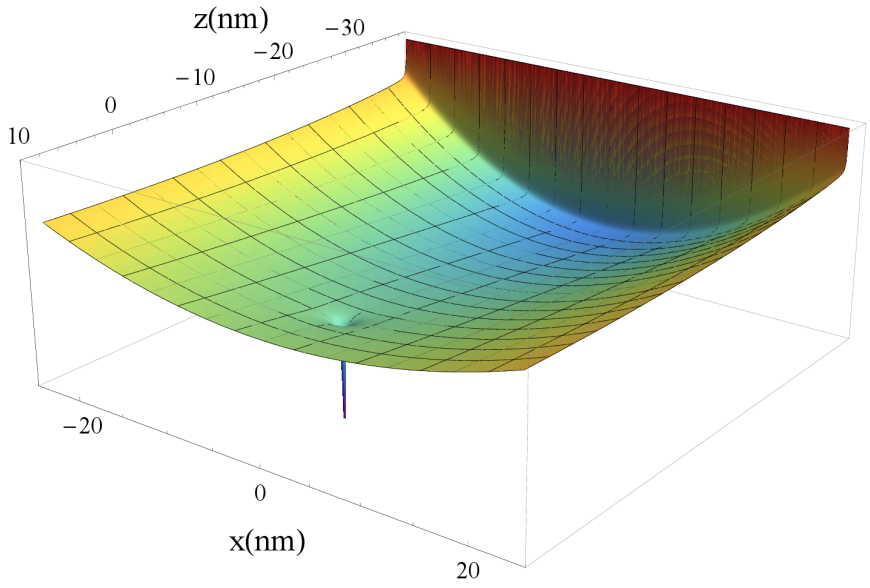

FIG. S1: A three dimensional plot of the two-well potential in Eq. S13, that binds the quantum dot electron at the interface with the oxide and the donor electron in the region close to the implanted dopant Bi atom, in the $x-z$ ($y=0$) plane. The origin of our coordinate system resides at the position of the Bi nucleus, while $z=-d$ corresponds to the interface plane. An electric field $F=20\,\mathrm{kV/cm}$ and a donor depth $d=38\,\mathrm{nm}$ are assumed.

EMT fails. Our theory for the donor state has been tested in Ref. [14] to yield good agreement with experimental Stark shifts of the spin Si:Bi spectrum. The donor wavefunction is there given by

$$\psi_D = \sqrt{\frac{2}{3}} \sum_{i=x,y,z} F_i^D(\mathbf{r}) \cos(\mathbf{k}_{0i}\cdot\mathbf{r}) u_i(\mathbf{r}), \tag{S14}$$

where the functions $u_i(\mathbf{r})$ are the lattice periodic parts of the Bloch eigenstates of the undoped silicon layer relative to each conduction band minimum $\mathbf{k}_{0i}$, and the anisotropic envelopes F^D are defined e.g. as:

$$F_z^D = N_D \left[\mathrm{e}^{-\sqrt{\frac{x^2+y^2}{a_s^2}+\frac{z^2}{b_s^2}}} + \beta\, \mathrm{e}^{-\sqrt{\frac{x^2+y^2}{a_l^2}+\frac{z^2}{b_l^2}}} \right], \tag{S15}$$

with different pairs of Bohr radii distinguishing the short (a_s, b_s) from the long (a_l, b_l) range hydrogen-like decay, with a relative weight β (N_D is a normalization factor). In the regime of donor depths and electric fields of interest here, the donor state can be assumed, to very high precision, to coincide completely with the bulk ground eigenstate, which is constructed from an equal superposition of the Bloch functions of all the six degenerate valleys.

The issues due to the valley degeneracy of the silicon conduction band are completely taken into account for the donor state, while we assume that the interface state resides in only one of the two $\hat{z}$-valleys combinations (namely, the symmetric one) that are almost degenerate close to the interface. Such degeneracy is known to be removed by the z-confinement provided by the Si/SiO_2 boundary and the electric field [16], with splittings as large as ≈ 1 meV that increase linearly with the applied field F [17], but a complete theory of the interplay of those effects will depend crucially on the details of the device. However, since the inter-valley coupling at the interface is not as strong as for a bulk donor, a more refined description would only provide the correct superposition of the two valleys that constitutes the orbital interface ground state, something that will not change qualitatively the analysis below. In fact, our calculations provide a worst case scenario, that is well suited to the feasibility study we are aiming at: the oscillations in $J(d)$ are maximal if the orbital state is an equal weight superposition of z valleys, so that the spatial dependence of the dot wavefunction is exactly in (anti-)phase with the donor one. Due to the roughness of the interface, for example, it is likely that other combinations of the two valleys, with different weights, correspond to the actual dot ground state: out-of-phase valley interference would then be able to reduce the large oscillations calculated here.

The envelope of the dot electron wavefunction is calculated via a variational optimization of its on-site ground binding energy, as determined by the potential in Eq. S13. Based on the strong similarity of the interface well with the exact solvable problem of an infinite triangular well, it has been proposed that a good *ansatz* for the interface envelope should resemble an Airy function [15]

along the z axis, while a Gaussian confinement is well suited to the $x-y$ confinement:

$$\psi_I = \sqrt{2}\cos[k_0(z+d)]\; u_{\mathbf{k}_{0z}}(\mathbf{r}) F_z^I(\mathbf{r}),$$
$$F_z^I(\mathbf{r}) = N_I (z+d)^2 e^{-\alpha(z+d)/2} e^{-\beta^2\rho^2/2}, \tag{S16}$$

where $5/\alpha$ gives the typical spread of the wavefunction in the $\hat{z}$ direction, while $2/\beta$ represents its extent in $x-y$ plane (N_I is a normalization factor). We solve variationally for the ground eigenstate and eigenvalue by optimizing α and β as a function of F and the donor depth d. In fact, even if the donor is implanted as deep as ~ 40 nm from the interface, the screened Coulomb attraction from the Bi nucleus affects the dot state in a non-negligible way. It provides a strong enough binding in the (001) plane that the transverse extent of the dot electron amounts to a radius of ≈ 25 nm, which already matches the lengthscales of experimental quantum dot engineering. As a consequence, ω_0 is neglected in our calculations.

The range of magnitudes of the exchange splittings that we need sets rather stringent requirements: if the dot is not tightly confined ($E_I \approx -12$ meV, F≈ 4 kV/cm), then the donor should be as deep as ~ 40 nm. If larger voltage gates are established, then the donors should be positioned closer to the interface, which is harder to realize, and the more efficient hybridization between donor and dot states combined with higher fields will make donor ionization more likely.

We use the Heitler-London method [18] to calculate the difference between the two lowest eigenvalues of the double electron problem. Within this scheme, the states are the orthonormalized symmetric and antisymmetric orbital superpositions of the product of two single electron functions ψ_I and ψ_D:

$$\Psi(\mathbf{r}_1,\mathbf{r}_2)_\pm = \frac{1}{\sqrt{2(1\pm S^2)}}(\psi^D(\mathbf{r}_1)\psi^I(\mathbf{r}_2) \pm \psi^D(\mathbf{r}_2)\psi^I(\mathbf{r}_1)). \tag{S17}$$

In Eq. S17 $\mathbf{r}_1, \mathbf{r}_2$ are the spatial coordinates of electron 1 and 2, respectively, and $S = \langle\psi^D|\psi^I\rangle$ is the overlap of the single-electron ground states. Exchange splittings are plotted in Fig. 4 in the main text as a function of the donor depth, and in Fig. S2 as a function of the applied field F. We use high precision numerical calculations to estimate the highly oscillatory

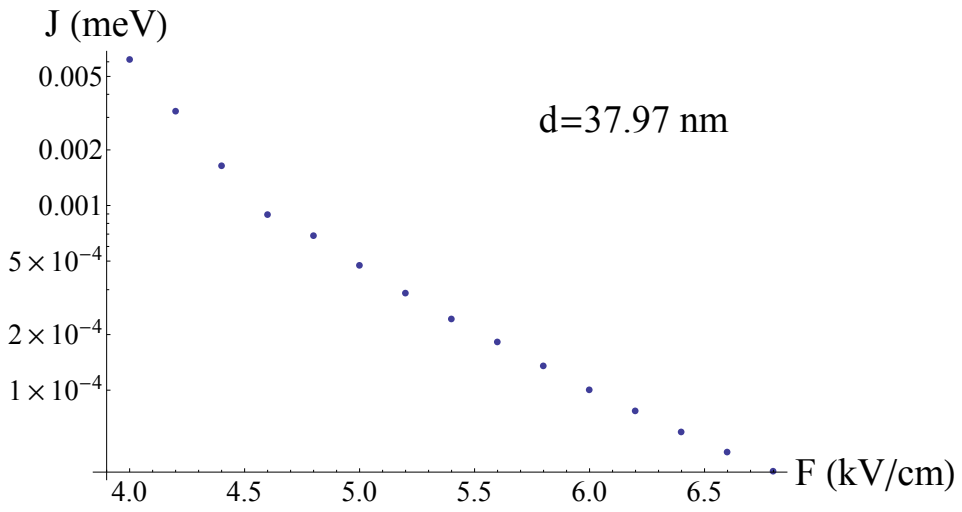

FIG. S2: Donor/dot exchange splittings as a function of the applied field: as F increases the dot is more localized at the interface, thus the interaction decreases. The control is very efficient: tuning the field by less than 3 kV/cm allows one to switch J 'off' by two orders of magnitude. A donor depth of $d = 37.97$ nm is assumed, but the same trend would be followed for any position of the Bi nucleus. At smaller fields the influence from the Coulomb attraction from the Bi impurity is still significant, and it affects the confinement of the dot state; then, from $F \gtrsim 4.5$ kV/cm, J becomes relatively less sensitive to the applied field, as the interface well is now more strongly established.

integrals involved in the calculation of the exchange coupling. The largest ratio between each $J(d)$ maximum and the next closest minimum is ≈ 0.01 for all the implantation depths considered here. The state-of-the-art implantation processes for donors in silicon allow a precision of ≈ 1 nm in the depth of the impurities (for example, a very shallow implant followed by low-temperature overgrowth [19]), which would correspond to several oscillations, and an estimated relative spread of maximum to minimum J values of 1:200. We remark that a different crystallographic direction could be chosen for engineering the quantum dots, which could reduce the strength of the oscillations in $J(d)$: for example, if the donor and the dot were separated along one [011] axis, then the interface ground state would be a combination of y and z valleys, but only the F_z components of the exchange would oscillate with d. However, the two-fold valley degeneracy discussed before would then

include more states. While the degeneracies would be very likely broken by the confinement and the interface roughness, the dot state would nonetheless be more liable to couple to excited orbital states, which would cause information leakage.
Let us highlight that the J values presented here would be completely robust against small displacements of the nominal donor position in the plane transverse to the donor/dot separation: no extra oscillation would take place if the donor and the dot are not completely aligned vertically, since the interface state is only made up of z valleys. This feature contrasts the behaviour of the exchange coupling between two neighbouring donors examined in Ref. [18], where all the valleys contribute to the interference, and thus J is sensitive to displacements along any spatial direction.

S4. THE LOGICAL HILBERT SPACE

In Sec. S2 we have selected the donor and the magnetic field regime of interest, and shown that they come out as the only natural option for the purposes of exploiting clock transitions. Let us now clarify to what extent the situation is changed after involving a dot electron that is able to interact with a Si:Bi system. Of course the Hilbert space of all the possible combinations of $I = 9/2$, $S_{\text{donor}} = 1/2$ and $S_{\text{dot}} = 1/2$ spin states is now 40-dimensional, and is governed by the Hamiltonian

$$H = \gamma_e \mathbf{B}_0 \cdot \mathbf{S}_{\text{donor}} - \gamma_n \mathbf{B}_0 \cdot \mathbf{I} + A\,\mathbf{S} \cdot \mathbf{I} + \gamma_e \mathbf{B}_0 \cdot \mathbf{S}_{\text{dot}} + J \mathbf{S}_{\text{donor}} \cdot \mathbf{S}_{\text{dot}}, \tag{S18}$$

where J is the exchange coupling between the two electron spins. This can be increased from zero – when the electron wavefunctions do not overlap much – by locally tuning the dot confinement gate voltage, causing the dot electron density to be pulled towards the implanted impurity.

With $J = 0$, let us consider the hybridized eigenstates of the donor/dot system governed by the Hamiltonian in Eq. S18: as a result of the degeneracy point between the dot and the donor clock transition, the following 'allowed' (A) and 'forbidden' (F) pairs of states cross close to the sweet spot identified in Sec. S2:

$$\begin{array}{l} |1\rangle^A = (\cos\frac{\theta_{-3}}{2}|1/2,-7/2\rangle + \sin\frac{\theta_{-3}}{2}|-1/2,-5/2\rangle) \otimes |\downarrow\rangle_{\text{dot}}, \\ |2\rangle^A = (-\sin\frac{\theta_{-4}}{2}|1/2,-9/2\rangle + \cos\frac{\theta_{-4}}{2}|-1/2,-7/2\rangle) \otimes |\uparrow\rangle_{\text{dot}}, \\ |1\rangle^F = (-\sin\frac{\theta_{-3}}{2}|1/2,-7/2\rangle + \cos\frac{\theta_{-3}}{2}|-1/2,-5/2\rangle) \otimes |\uparrow\rangle_{\text{dot}}, \\ |2\rangle^F = (\cos\frac{\theta_{-4}}{2}|1/2,-9/2\rangle + \sin\frac{\theta_{-4}}{2}|-1/2,-7/2\rangle) \otimes |\downarrow\rangle_{\text{dot}}. \end{array} \tag{S19}$$

However, when the wavefunctions of the two electrons considered here overlap significantly, i.e. when $J \neq 0$, these eigenstates are mixed, and the corresponding spectra are affected in two qualitatively different ways: the states $|1\rangle^A$ and $|2\rangle^A$ go through an avoided crossing if $J \neq 0$, as shown in the inset of Fig. 2 in the main text, while $|1\rangle^F$ and $|2\rangle^F$ simply cross each other. In fact, while the only nonzero matrix elements contributed by $J\mathbf{S}_{\text{donor}} \cdot \mathbf{S}_{\text{dot}}$ occur between electronic spin pairs with the same $\mathbf{S}_{\text{donor}}+\mathbf{S}_{\text{dot}}$ projection, the orthogonality of the nuclear spin eigenstates prevents any finite matrix elements that do not involve the same nuclear spin projection on both states. For these reasons, ${}^A\langle 1|J\mathbf{S}_{\text{donor}} \cdot \mathbf{S}_{\text{dot}}|2\rangle^A \neq 0$, while ${}^F\langle 1|J\mathbf{S}_{\text{donor}} \cdot \mathbf{S}_{\text{dot}}|2\rangle^F = 0$. Thus if we induce an adiabatic evolution where the two pairs $\{|1\rangle^A, |2\rangle^A\}$ and $\{|1\rangle^F, |2\rangle^F\}$ are swept through their (anti-)crossing point, the nuclear state fundamentally determines the occurrence of a population transfer in the first case and nothing but phase accumulation in the second.

Let us clarify this reasoning: we enlarge the computational basis of our system to a combination of three qubits, which are shown schematically in Fig. 3 in the main text:

$$\begin{array}{ll} |1\rangle \equiv |000\rangle = |\downarrow\rangle_{\text{dot}} |-, m=-3\rangle_{\text{donor}} & |5\rangle \equiv |100\rangle = |\uparrow\rangle_{\text{dot}} |-, m=-3\rangle_{\text{donor}} \\ |2\rangle \equiv |001\rangle = |\downarrow\rangle_{\text{dot}} |-, m=-4\rangle_{\text{donor}} & |6\rangle \equiv |101\rangle = |\uparrow\rangle_{\text{dot}} |-, m=-4\rangle_{\text{donor}} \\ |3\rangle \equiv |010\rangle = |\downarrow\rangle_{\text{dot}} |+, m=-4\rangle_{\text{donor}} & |7\rangle \equiv |110\rangle = |\uparrow\rangle_{\text{dot}} |+, m=-4\rangle_{\text{donor}} \\ |4\rangle \equiv |011\rangle = |\downarrow\rangle_{\text{dot}} |+, m=-3\rangle_{\text{donor}} & |8\rangle \equiv |111\rangle = |\uparrow\rangle_{\text{dot}} |+, m=-3\rangle_{\text{donor}}\,. \end{array} \tag{S20}$$

When an exchange interaction is turned on between the dot and the donor electron spins, an off-diagonal coupling is induced between states $|4\rangle$ and $|6\rangle$, while the allowed/forbidden selectivity just explained prevents a similar coupling between states $|3\rangle$ and $|5\rangle$ [21]. Thus, only if the state is of form $|xx1\rangle$ - i.e. the NMR qubit is in state '1' - can a swap be induced between the dot and the ESR qubit by sweeping the magnetic field B_0 through a $E_4 - E_6$ degeneracy with a pulsed exchange coupling, as further detailed in the next Section. The same time evolution, on the other hand, would not swap Dot and ESR states if the state is $|xx0\rangle$. Such evolution would thus correspond to a three-qubit Fedkin gate [20], which (as shown in Fig. 4(a) in the main text) can be achieved with high fidelity across the wide range of J couplings expected from the non-exact positioning of the implanted donors.

S5. ADDRESSABLE ADIABATIC INFORMATION TRANSFER BETWEEN THE DONOR AND THE DOT

In this Section we present the kind of dynamics that would lead to a robust SWAP of the two quantum states $|4\rangle$ and $|6\rangle$: we restrict ourselves to the basis of the four states $|2\rangle, |6\rangle, |4\rangle, |8\rangle$ defined in Eq. S20, which correspond to the configuration with NMR qubit fixed to '1', as explained before. As shown in Fig. 4(b) in the main text, we propose initializing the DC magnetic field at a point away from the anticrossing, where the states are not mixed. This is a 'quiet' phase configuration at a field of $B_0(-t_0) = B_0^* - \Delta B_0$, where B_0^* marks the $E_4 - E_6$ degeneracy point and $\Delta B_0 \approx 5\,\mathrm{mT}$. The field is then swept through the anti crossing and beyond, up to $B_0(+t_0) = B_0^* + \Delta B_0$. The coil currents that generate the DC magnetic field could heat the device unacceptably if the sweep rate is too fast, thus we assume that a sweep of $10\,\mathrm{mT}$ is attainable within a $2t_0 \approx 2\,\mu\mathrm{s}$ time interval. This is the fundamental limitation on the speed of the proposed gate.

In the meantime, the exchange coupling is turned on adiabatically from its quiet value $J(-t_0)$, that is much smaller than the initial detuning $|E_4(-t_0) - E_6(-t_0)| \approx 140\,\mathrm{MHz}$, to some maximum $J_{\max}$, which is achieved at $t = 0$ when $E_4(0) = E_6(0)$, and then back to the quiet stage (see Fig. 4(b)). As explained in the main text, this operation can be performed easily by increasing the extent of the electron dot wavefunction via modification of the back gate voltage: Fig. S2 quantifies the degree of J tunability, showing that the coupling can easily be increased by three orders of magnitude if we decrease the electric field that confines the dot by 4 kV/cm. The qubit states at $t = -t_0$ will adiabatically follow the instantaneous eigenstates of the time-dependent evolution, hence if the coupling is strong enough during a sufficient interval of time, a strong population transfer between the diabatic $|4\rangle$ and $|6\rangle$ states will take place. More precisely, the time evolution operator induced by the dynamics just outlined in the four-states basis above will read as the block matrix

$$\begin{pmatrix} \exp[-i\int_{-t_0}^{t_0} dt E_2(t)/\hbar] & 0 & 0 \\ 0 & \exp[-i\int_{-t_0}^{t_0} dt (E_6(t)+E_4(t))/2\hbar] U(+t_0,-t_0) & 0 \\ 0 & 0 & \exp[-i\int_{-t_0}^{t_0} dt E_8(t)/\hbar] \end{pmatrix}, \tag{S21}$$

where the eigenergies are: $E_2(t) = E_{-4}^{2-}(t) - B_0(t)\frac{\gamma_e}{2} - \frac{J(t)}{4}\cos\theta_{-4}(t)$, $E_8(t) = E_{-3}^{2+}(t) + B_0(t)\frac{\gamma_e}{2} + \frac{J(t)}{4}\cos\theta_{-3}(t)$, $E_6(t) = E_{-4}^{2-}(t) + B_0(t)\frac{\gamma_e}{2} - \frac{J(t)}{4}\cos\theta_{-4}(t)$ and $E_4(t) = E_{-3}^{2-}(t) - B_0(t)\frac{\gamma_e}{2} - \frac{J(t)}{4}\cos\theta_{-3}(t)$, and the two-state transfer matrix $U(+t_0,-t_0)$ is

$$U(t_0,-t_0) = \begin{pmatrix} a\,e^{i\psi} & \sqrt{1-a^2}\,e^{i\phi} \\ -\sqrt{1-a^2}\,e^{-i\phi} & a\,e^{-i\psi} \end{pmatrix}, \tag{S22}$$

where a is a real number, and ψ and ϕ are two real phases. Importantly, though at any time $J(t)$ can change by two orders of magnitude across all the parallel donor/dot pairs (as shown in Fig. 4(a) in the main text), it always has the same time dependent profile. The goal is to achieve high population transfer fidelities, i.e. to make a small enough, over this large range of J couplings, so that $U(-t_0,t_0)$ should resemble a SWAP operation (times a compensable Z-phase gate) irrespective of the strength of the donor/dot coupling. An adiabatic evolution where the exchange is pulsed slowly with respect to the magnitude of the initial detuning, $\hbar\dot{J}(t) \ll (140\,\mathrm{MHz})^2$, allows such an insensitivity of the time propagator to the J coupling.

Calculations of the exact time evolution of the system in the adiabatic regime just defined, with $\Delta(t) = -\Delta_0(\frac{t}{t_0}), -t_0 \leq t \leq t_0$, $t_0 = 2\,\mu\mathrm{s}$ and $J(t) = J_0(1-\exp[(|t|-t_0)/\sigma])$, where $\sigma = 0.9\,\mu\mathrm{s}$ sets a realistic timescale for tuning the back gate voltage, leads to the transfer population fidelities $|U_{12}(+t_0)|^2$ shown in Fig. 4(a) in the main text. Fidelities higher than 99.9%, thus within the fault tolerance set by the surface code, can be achieved within $2\,\mu\mathrm{s}$ for all the donor/dot pairs addressed by a local exchange-tuning.

However, the realization of a Dot/NMR CNOT gate as proposed in Eq. 1 in the main text would not follow immediately if the Dot/ESR 'SWAP' $\mho$ is implemented by the time evolution defined in Eqs. S22 and S21. The reason for such failure lies in the presence of the J-dependent phase $\phi \neq 0$, which implies that the operator in Eq. S22 has entangling power: its action would not be limited to SWAPping the quantum states involved. This problem is solved by the longer sequence illustrated in Fig. 4(b) in the main text, that combines the time evolution in Eq. S22 with a 'phase-erasing' operation. The only extra ingredients required by this simple recipe are selective Rabi resonant pulses that can be easily achieved, one after the other, via a transverse ac magnetic field $\mathbf{B}(t) = B_1(\cos(\omega t)\hat{\mathbf{x}} - \sin(\omega t)\hat{\mathbf{y}})$, with high fidelity for µs gating times. It is easy to verify numerically that the result of this updated sequence is now written as

$$\mho \equiv e^{-i\int dt(E_6+E_4)/\hbar} \begin{pmatrix} e^{-i\int(E_2+E_8-E_6-E_4)/\hbar} & 0 & 0 & 0 \\ 0 & ae^{i\theta} & -\sqrt{1-a^2} & 0 \\ 0 & \sqrt{1-a^2} & ae^{-i\theta} & 0 \\ 0 & 0 & 0 & e^{-i\int(E_2+E_8-E_6-E_4)/\hbar} \end{pmatrix}, \tag{S23}$$

where the phase ϕ has now disappeared. Straightforward matrix multiplication shows that the complete sequence in Eq. 1 in the main text, assuming for simplicity a perfect Dot/ESR transfer ($a = 0$), leads to the following time propagator in the complete basis of Eq. S20:

$$-i \begin{pmatrix} \mathcal{I} & 0 & 0 & 0 \\ 0 & \boxed{\begin{matrix} 0 & 1 \\ 1 & 0 \end{matrix}} & 0 & 0 \\ 0 & 0 & \boxed{\begin{matrix} 0 & 1 \\ 1 & 0 \end{matrix}} & 0 \\ 0 & 0 & 0 & \mathcal{I} \end{pmatrix}. \tag{S24}$$

This is seen to coincide with the desired surface code CNOT, when restricted to the degrees of freedom that effectively host the data and measurement qubits, namely the states with the ESR qubit being initialized to '0': $|1\rangle, |2\rangle, |5\rangle, |6\rangle$.

[1] P. Harvey-Collard, G. A. Ten Eyck, J. R. Wendt, T. Pluym, M. P. Lilly, M. S. Carroll, and M. Pioro-Ladriere, in *Bulletin of the APS* **60** (2015).
[2] J. C. Li *et al.*, ECS Transactions **50**, 1047 (2013).
[3] J. M. Elzerman, R. Hanson, L. H. W. van Beveren, B. Witkamp, L. M. K. Vandersypen, and L. P. Kouwenhoven, Nature **430**, 431 (2004).
[4] A. Morello, J. J. Pla, F. A. Zwanenburg, K. W. Chan, K. Y. Tan, H. Huebl, M. Möttönen, C. D. Nugroho, C. Y. Yang, J. A. van Donkelaar, A. D. C. Alves, D. N. Jamieson, C. C. Escott, L. C. L. Hollenberg, R. G. Clark, and A. S. Dzurak, Nature **467**, 687 (2010).
[5] C. C. Lo, M. Urdampilleta, P. Ross, M. F. Gonzalez-Zalba, J. Mansir, S. A. Lyon, M. L. W. Thewalt, and J. J. L. Morton, Nature Materials **14**, 490 (2015).
[6] C. Yin, M. Rancic, G. G. de Boo, N. Stavrias, J. C. McCallum, M. J. Sellars, and S. Rogge, Nature **497**, 91 (2013).
[7] T. A. Fulton and G. J. Dolan, Phys. Rev. Lett. **59**, 109 (1987).
[8] M. Field, C. G. Smith, M. Pepper, D. A. Ritchie, J. E. F. Frost, G. A. C. Jones, and D. G. Hasko, Phys. Rev. Lett. **70**, 1311 (1993).
[9] R. E. George, W. Witzel, H. Riemann, N. V. Abrosimov, N. Nötzel, M. L. W. Thewalt, and J. J. L. Morton, Phys. Rev. Lett. **105**, 067601 (2010).
[10] G. Wolfowicz, A. M. Tyryshkin, R. E. George, H. Riemann, N. V. Abrosimov, P. Becker, H.-J. Pohl, M. L. W. Thewalt, S. A. Lyon, and J. J. L. Morton, Nature Nanotechnology **8**, 561 (2013).
[11] M. H. Mohammady, G. W. Morley, A. Nazir, and T. S. Monteiro, Phys. Rev. B **85**, 094404 (2012).
[12] M. H. Mohammady, G. W. Morley, and T. S. Monteiro, Phys. Rev. Lett. **105**, 067602 (2010).
[13] G. W. Morley, M. Warner, A. M. Stoneham, P. T. Greenland, J. van Tol, C. W. M. Kay, and G. Aeppli, Nature Materials **9**, 725 (2010).
[14] G. Pica, G. Wolfowicz, M. Urdampilleta, M. L. W. Thewalt, H. Riemann, N. V. Abrosimov, P. Becker, H.-J. Pohl, J. J. L. Morton, R. N. Bhatt, S. A. Lyon, and B. W Lovett, Phys. Rev. B **90**, 195204 (2014).
[15] M. J. Calderon, B. Koiller, and S. Das Sarma, Phys. Rev. B **75**, 125311 (2007).
[16] M. J. Calderón, B. Koiller, X. Hu, and S. Das Sarma, Phys. Rev. Lett. **96**, 096802 (2006).
[17] A. L. Saraiva, M. J. Calderón, R. B. Capaz, X. Hu, S. Das Sarma, and B. Koiller, Phys. Rev. B **84**, 155320 (2011).
[18] G. Pica, B. W. Lovett, R. N. Bhatt, and S. A. Lyon, Phys. Rev. B **89**, 235306 (2014).
[19] B. E. Kane, Fortschr. Phys. **48**, 1023 (2000).
[20] E. Fredkin and T. Toffoli, International Journal of Theoretical Physics **21**, 219 (1982).
[21] For completeness, we note that a similar coupling would be induced between states $|1\rangle$-$|7\rangle$, whose energy splitting is however very large, about 10 GHz, at all times during the sweeping of the magnetic field B_0. Thus no significant SWAP would be induced between such states even if the J coupling is pulsed.